CYCLIC KNEE TESTING MACHINE

A Project Report

submitted by

SUBHAM SWASTIK SAMAL

in partial fulfilment of the requirements
for the award of the degree of

BACHELOR OF TECHNOLOGY

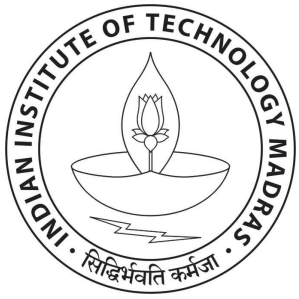

DEPARTMENT OF MECHANICAL ENGINEERING
INDIAN INSTITUTE OF TECHNOLOGY MADRAS.

MAY 2020

THESIS CERTIFICATE

This is to certify that the thesis titled **"CYCLIC KNEE TESTING MACHINE"**, submitted by **Subham Swastik Samal**, to the Indian Institute of Technology, Madras, for the award of the degree of **Bachelor of Technology**, is a bonafide record of the research work done by him under our supervision. The contents of this thesis, in full or in parts, have not been submitted to any other Institute or University for the award of any degree or diploma.

Dr. Sujatha Srinivasan
Research Guide
Professor
Dept. of Mechanical Engineering
IIT-Madras, 600 036

Place: Chennai

Date: 19th April 2020

ACKNOWLEDGEMENTS

I would like to express my sincere gratitude to my supervisor Dr. Sujatha Srinivasan for introducing the present topic and guiding me thoughtfully and efficiently through this project, giving me an opportunity to work at my own pace along my lines, while providing me with very useful directions whenever necessary.

I would also like to thank Dr. Javeed Shaikh Mohammed and Mr. Sudheesh Subramanian for patiently helping me and providing constant support throughout the project work. I would also like to thank the members of R2D2 Lab, IIT Madras, for helping to carry out my research.

ABSTRACT

KEYWORDS: Polycentric knee; Longevity; Mechanisms; Prostheses

The document summarises my Bachelor's Thesis Project involving the ideation and design of a mechanism, which can operate to test the walking longevity of prosthetic knee joints. Prosthetic knee joints are designed to mimic the flexion and extension of the anatomical knee joint as the user walks. Usually, the prosthetic knee works together with a prosthetic shank and foot to achieve a smooth gait pattern. The mechanism devised can be used to run the prosthetic knees continuously to determine the number of cycles they will last, and thus the distance they can be used safely. 3-D modelling of the mechanism has been done by taking appropriate dimensions and making reasonable approximations in CREO Parametric 6.0. Industrial components like bearings, linear guides, fasteners, etc. have been selected based on the forces and torques acting, and have been incorporated into the CAD model. Finite Element Analysis has been done in ANSYS to ensure the safety of the mechanism. The report discusses the implementation of these tasks and the major results in detail.

TABLE OF CONTENTS

LIST OF TABLES

LIST OF FIGURES

NOTATION

s	Shortest link in a four bar linkage
l	Longest link in a four bar linkage
ψ	Angle range of rocker
H	Vertical distance between crank-motor joint and rocker-frame joint
α	Angle made by crank with horizontal plane when rocker is vertical
$(V_i)_j$	Velocity of link j along i direction
$(a_i)_j$	Acceleration of link j along i direction
ω_i	Angular velocity of link i
α_i	Angular acceleration of link i
m_i	Mass of element i
$(F_{ij})_k$	Component of the force acted by link i on j along k direction
T_{ij}	Torque acted by link i on j
R_{ij}	Vector starting from CoG of link j till the junction of i and j
I_k	Moment of inertia of link k
g	Acceleration due to gravity
σ_y	Yield stress

CHAPTER 1

INTRODUCTION

1.1 Prosthetic Knees and Mechanisms

Prosthetic knees are designed to mimic the bending (flexion) and swinging (extension) of the anatomical knee joint as a user walks. From advanced computer-controlled components to simple locking joints, the prosthetic knee works together with the prosthetic foot and socket to achieve a smooth gait pattern. Based on their mechanism, all prosthetic knees fall into one of two categories, single-axis or polycentric (multiple axes.) A single-axis knee is one in which there is one axis of rotation, like a door hinge and swings forward and backward. Single-axis knees typically require greater muscle strength because the centre of rotation or point at which the knee moves is fixed. Polycentric knees have more than one axis of rotation. These knees also move in the forward and backward direction, but there are more moving parts and create a more stable knee joint due to a moving centre of rotation. These knees are excellent for those with a knee disarticulation or longer transfemoral residual limb because owing to their design when they bend (flex), they shorten during the swing phase.[5]

1.1.1 Single-Axis Knees

Single-axis knees are basic knees that bend freely. The amputees must rely on their muscle control for stability. The single-axis constant friction knee is generally used by children who have a lower centre of gravity or for users with excellent musculature control that walk at a single speed. For exoskeletal knees, an extension strap made of elastic may be added to the front of the prosthesis to aid the knee in kicking forward.

- **Mechanism**: This is a simple hinge type knee. During the flexion/extension, these articulations execute a simple rotation around the knee axis. They are of simple design, and their easy alignment responds to the rules of mechanics. There are exoskeletal

Figure 1.1: Single-Axis knee[22]

and endoskeletal single-axis knees. Both versions could have manual or automatic blocking of the flexion for users with poor muscle power. The knees without blocking can be used for regular prosthetic fitting of amputees with adequate muscle control and/or in situations of limited economic resources.[8]

- **Advantages**: They are very simplistic in design, very light and economical. Since they have fewer moving parts due to their simplicity, they are durable.
- **Disadvantages**: Due to the simplicity, the individual has to use their own muscle power in the limb to keep the knee stable with heel contact and standing. Since the distance from centre of rotation to toe is fixed during the swing phase, there is a higher risk of stumbling. Also, they are less adaptable to different walking speeds and become less stable as they wear.
- **Additional components**: A manual lock can be added to give more stability in standing. A constant friction control can also be added, which will prevent the leg from swinging through very quickly.

1.1.2 Polycentric Knees

Polycentric knees are suitable for a wide range of amputees. Various versions are ideal for amputees who cannot walk securely with other knees, have knee disarticulation or bilateral leg amputations, or have long residual limbs.

Figure 1.2: Polycentric knee[22]

- **Mechanism**: This knee has multiple axes of rotation. Polycentric knees can be four-bar, six-bar or seven-bar knees. Knees of the most frequent use are of 4-axes (or 4-bars). Without giving importance to the number of axes, the knees of poly-axial design have one thing in common - the Instant Centre of Rotation (ICR) is situated much higher and posterior to the mechanical axes when the knee is in extension. To localize the ICR of a polycentric knee, we need to extend virtually the centre lines of the lateral bars towards proximal - the intersection of those lines will indicate the ICR. Standard polycentric knees have a single walking speed, but when a manufacturer includes pneumatic or hydraulic features, the user will be able to vary their walking speed.[8][9]

- **Advantages**: It is very versatile in terms of stability and could be adjusted to be extremely stable when the user goes into the stance phase, but at the same time allow easy swing and allows sitting down with a bent knee. Due to the multiple axes and the ICR, the prosthetic length "shortens" at the start of toe-off and allows for foot clearance, thus reducing the risk of stumbling. It is suitable for users with the potential to be independent with the prosthesis in their home and community.[11]

- **Disadvantages**: They are generally larger and heavier than single-axis knees. More parts that need servicing. Most polycentric knees do not have stance flexion resistance and, therefore, cannot yield during sitting, ramps, or stairs. A person with a knee that is not controlled by a microprocessor needs to actively generate a knee extension moment in the stance phase to prevent the knee from buckling and cause the person to fall down.

1.1.3 Need for prosthetics testing

During walking cycle, a knee joint prosthesis is subjected to cyclic loading which can cause failure due to fatigue, making it necessary to evaluate their life before recommending to users. Prolonged usage of prosthetic knees could result in loosening of various joints and springs in the knees, fatigue failure of components like bearings, pins and bolts, buckling and wearing of joint linkages, etc. These could lead to users facing problems such as rotation of pylon tube during walking, hyper-extension of the knee during extension and noise during walking. Due to lack of active control, such problems could result in loss of stability and balance of the user while walking, which could lead to discomfort and accidents. Therefore, it is necessary to test the life of the prostheses i.e. the minimum distance the user can walk without facing these complications.

1.2 Literature Review

A traditional evaluation criterion for lower limb prostheses mostly depend on the subjective feelings of the amputees instead of quantitative performance. These evaluations involved questionnaires to be filled out by the prosthetic users from time to time. The questionnaires are usually developed with the aid of professionals, including therapists, prosthetists and engineers, working in the field.[16][10][12][4] These questionnaires address numerous factors such as appearance, fatigue, stability, fit, discomfort and pain, types of activities, and physical environments. While such tests do provide valuable insights,they are time consuming and tedious. This is especially because issues like loosening of joints and springs in the knees, noise, failure of components like bearings, pins and bolts etc. usually take months to appear.

The earliest methods of testing prostheses included quasi-static devices, in which the knee can be positioned at a desired knee-flexion angle and then loaded with forces and torques. Compressive, torsional and hyperextensive loads were added using proper setups to calculate their strengths.[1][20]The major drawback of such quasi-static machines is the inability to dynamically simulate activities. With the development of FEA simulation in CAE softwares like ANSYS and CATIA, many researchers have used such tools to determine safety and life of prosthetic knees. Many research groups have presented such studies; the simplest studies considering the weight of the person, maximum knee joint force while walking, ground reaction forces etc. to perform a static

analysis.[7][6] A few others have proposed analysing for static and cyclic loading.[15] The static test guarantees that the prosthesis is able to sustain a random severe load that it may experience in its life, and its fatigue strength is proofed in the cyclic test. Some others have performed analysis for different positions of the gait cycle, using the loads on the knee joint at each configuration. [25][13] Such analyses are only suited for static activities like standing or activities which involve less motion. Since we can't formulate certain impact loads like when the knee hits the bump-stop at full extension at the end of swing phase, they aren't suitable for dynamic activities like walking. Besides, formulating these evaluations tend to get more complicated and inaccurate as the number of parts in the prosthesis increase.

Further advancement in technology with time led to the development of knee simulators, machines that can dynamically simulate the loads and motions on a complete set of prostheses. Some of the most advanced knee simulators have been developed since the turn of the century, some of which include the Purdue Mark II[18]/ Kansas Knee Simulator, Hannover Knee Simulator[21], New York Knee simulator[26], etc. These simulators can reproduce the natural dynamic loading on the knee as well as simulate athletic activities by inducing high loads and rapid motions. These simulators are usually multi-purpose; they are used for studying biomechanics of the knee joint for various activities by using cadaveric specimens and actuators to simulate muscle forces, testing the effects of partial and total knee replacements, and evaluate their wear characteristics, etc. Some of them even have setups to properly lubricate the joint and keep them at room temperature while they are in action. Thus, almost all of these knee simulators tend to have complex mechanisms with many actuators and sensors, and are unaffordable and heavy. Even though testing of prosthetic knee-life is possible in such simulators, it is not one of the primary purpose of their development.

Because of the above disadvantages of knee simulators, some researchers have come up with robotic mechanisms, which are specialized to test knee prosthesis. A testing mechanism proposed by a group of researchers from the USST, Shanghai[2] applies treadmill to simulate level walking of prosthetic leg. It also consisted of lifting air cylinders to simulate the gravity shift of human body and a motor to drive the hip joint.Kim and Oh[14] designed a motion platform, which used a large four-bar linkage mechanism to generate the vertical motion and swing of the thigh simulation mechanism. While the above methods can accommodate polycentric knees, one needs to modify

certain parameters in the controller before changing the knee model. For example, in the mechanism developed in USST, the lifting air cylinders have to be lifted to different heights for different knees. Therefore, the attempt in this project is to develop a simpler method for testing of prosthetic knees that can accommodate a variety of knee mechanisms.

1.3 Objectives and Scope

The objective of this project was to devise a standard setup for calculating the swing-phase life of prosthetic knees. Multiple knee systems were studied to ideate a common mechanism that could accommodate them. Normal walking gait in humans was studied to formulate a four-bar linkage system, whose rocker guides the motion of the shank. Kinematic and dynamic analyses were performed for the selection of various components and design of the experimental setup. Finite element analysis at potential weak locations has also been done, thus ensuring that the system can run for a long time without failure.

1.4 Organization of the report

The thesis is organized as follows: Chapter 1 discusses prosthetic knee mechanisms and available test simulators, the literature available on it and the objectives of this work. Chapter 2 proposes a mechanism for knee testing and describes the formulation of the four-bar mechanism that acts as a motion simulator of the prosthetic knees. Chapter 3 covers the motion and force analysis of the mechanism, which is necessary for the selection of motor and gearbox, and designing of the experimental setup or frame. Chapter 4 uses the previous analysis to select appropriate industrial components like bearings and linear guides. Chapter 5 presents the conclusions and the future course for carrying this work forward.

CHAPTER 2

PROPOSED MECHANISM

2.1 Mechanism Overview

The mechanism consists of a four-bar linkage system with a crank-rocker configuration. The crank is attached to a motor that rotates at a constant angular velocity. The shank (pylon) of the prosthesis is coupled to the rocker, and thus, the motion of the shank is identical to that of the rocker. The links are designed such that the motion of the rocker is similar to that of the tibia during the swing phase of a normal human gait cycle.

For polycentric knee models, the instantaneous centre of rotation (ICR) changes as the joint is rotated (flexed or extended) about the sagittal plane. Thus, at any point during the rotation, the ICR will have 2 degrees of freedom in the sagittal plane (horizontal and vertical). Therefore, two linear motion systems have been connected with the thigh (pylon) of the prosthesis to account for the motions in the 2 directions. The bushing allows vertical motion, while the linear guide system allows horizontal motion. Together, they account for free movement of the ICR without any constraints. If a single axis knee is fitted into the mechanism, rotating the crank will generate flexion and extension of the knee as well, but there will be no movement along the linear motion systems. It is also made sure that the joint of rocker and shank is positioned low enough to accommodate knee models of larger sizes.

In the mechanism shown in Fig 2.1, the degrees of freedom of the complete mechanism (along with the prosthesis fitted) is 1.
Gruebler's equation states that:

$$F = 3(n-1) - 2*l - h$$

where: F = total degrees of freedom

n = number of links (including the frame) = 8

l = number of lower pairs (one DOF) = 10

h = number of higher pairs (two DOF) = 0

So, no. of degrees of freedom in our mechanism = $3*(8-1) - 2*10 - 0 = 1$

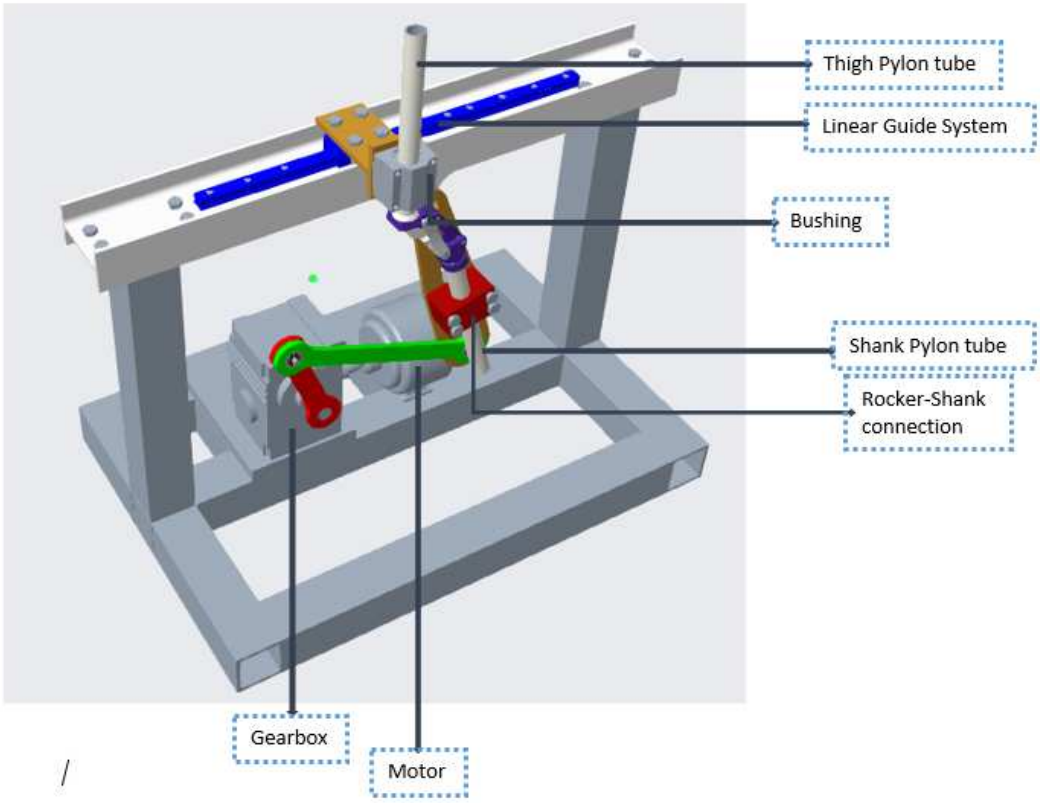

Figure 2.1: The proposed mechanism, when fitted with a prosthetic knee designed at R2D2 Lab, IIT Madras

2.2 Computation of link lengths for the four-bar linkage

2.2.1 Formulation

The proposed mechanism is a four-bar crank-rocker. Thus:

- The sum of lengths of shortest and longest links must be lesser than the sum of the other two link lengths ($l + s < p + q$)
- The crank link must be the shortest of all the links

The average walking speed (self-selected) of an adult human is about 1.3-1.4 m/s. For users with prosthetic knee joints, this is usually lower. The range of walking speed varies with the users, based on the knee design, and thus for prosthesis users in general, an average walking speed of 0.9-1.1m/s can be considered. At those speeds, based on the analysis of diagram in Figure 2.2, the ratio of time taken for flexion and extension in the swing phase is about 4:3. Thus, the 360^o rotation of the crank can be divided as:

- 210^o rotation for flexion of rocker from 0^o to 70^o.
- 150^o rotation for extension/retraction of the rocker.

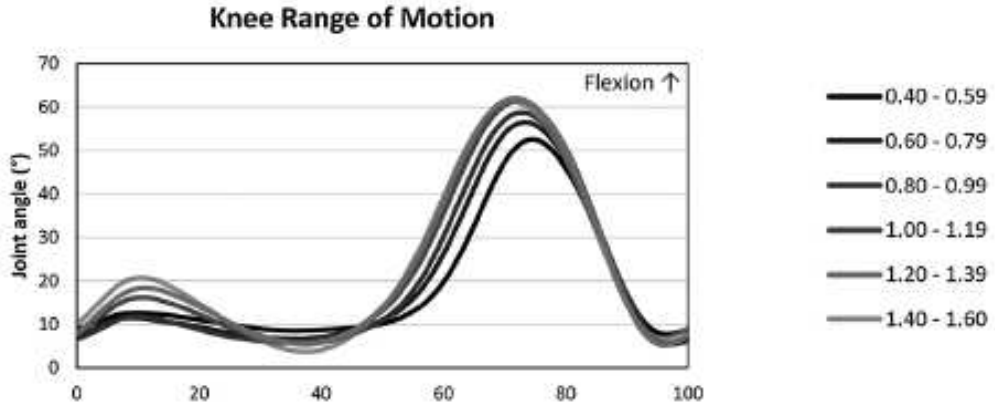

Figure 2.2: Sagittal plane knee joint angle during walking at various speeds (in m/s). Percentage of the gait cycle is shown on the X-axis. [19]

As in Figure 2.2, the maximum knee flexion angle during the swing phase is about $50^o - 63^o$ for various walking speeds. Thus, keeping a tolerance, the mechanism has been designed to flex the knee angle by 70^o. Since the shank is connected to the rocker of the four-bar mechanism, the rocker must have the range of $0^o - 70^o$ for rotation.

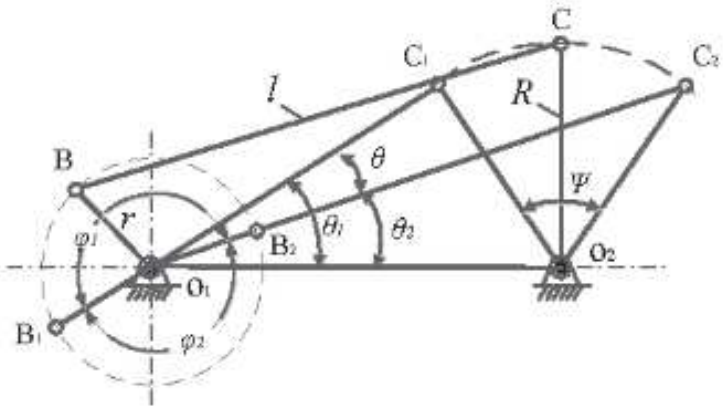

Figure 2.3: Standard procedure of designing crank-rocker mechanism

Figure 2.3 depicts the standard formulation of a crank-rocker mechanism[17]. For this system, $\psi = 70^o$ and $\theta = 30^o$. $O_1B_1C_1O_2$ represents the corresponding configuration in our mechanism when the knee joint is at complete extension. For simplicity in handling the entire model, the thigh pylon is made to align completely vertically in this configuration.

Based on the above parameters, our four-bar mechanism can be represented using the diagram below. The yellow, red and blue segments represent the crank, connecting rod and rocker, respectively. 'H' and 'α' are variables here. OO' is the horizontal distance between the two fixed points. These three parameters are introduced as they will be useful to build constraints, as explained later.

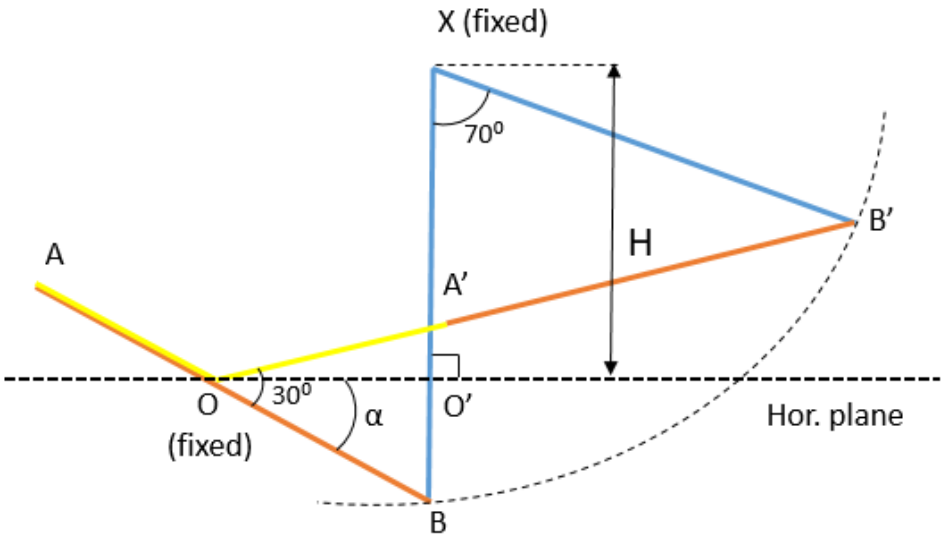

Figure 2.4: Extreme points of the four-bar mechanism

Let L_1, L_2 and L_3 be the lengths of the crank, connecting rod and rocker, respectively.

Thus: $(L_2 - L_1) * sin(\alpha) + L_3 = H$

$$(L_1 - L_2) * cos(\alpha + 30) - L_3 * sin(70) = OO'$$

$$(L_2 - L_1) * cos(\alpha) = OO'$$

$$(L_1 + L_2) * sin(\alpha + 30) + L_3 * cos(70) = H$$

Writing the above equations in Matrix form,

$$\begin{bmatrix} sin(\alpha) & 0 & 1 & 0 \\ 0 & cos(\alpha + 30) & -sin(70) & -1 \\ cos(\alpha) & 0 & 0 & -1 \\ 0 & sin(\alpha + 30) & cos(70) & 0 \end{bmatrix} * \begin{bmatrix} (L_2 - L1_) \\ (L_1 + L_2) \\ L_3 \\ OO' \end{bmatrix} = \begin{bmatrix} H \\ 0 \\ 0 \\ H \end{bmatrix}$$

$$\Rightarrow \begin{bmatrix} (L_2 - L_1) \\ (L_1 + L_2) \\ L_3 \\ OO' \end{bmatrix} = \begin{bmatrix} sin(\alpha) & 0 & 1 & 0 \\ 0 & cos(\alpha + 30) & -sin(70) & -1 \\ cos(\alpha) & 0 & 0 & -1 \\ 0 & sin(\alpha + 30) & cos(70) & 0 \end{bmatrix}^{-1} * \begin{bmatrix} H \\ 0 \\ 0 \\ H \end{bmatrix}$$

Thus, unless the transformation matrix is non-invertible, a pair of (α,H) will give a set of values for L_1, L_2, L_3 and OO'. These values can be positive or negative based on the input values of (α,H). They can also be very high or very small based on the inputs. Thus, it is necessary to devise an appropriate optimization technique. For this, a few more constraints need to be added.

2.2.2 Constraints

- If the horizontal distance between the motor-crank connection and the rocker-frame connection, i.e., OO' in the figure, is taken to be very less, then it could lead to interference. So, a lower limit of 15 cm was kept for that length.
- Mounting a motor to higher altitudes could be complicated. To ensure that the motor is placed at a lower height, a lower limit of 30 cm was kept for the vertical distance between the motor-crank connection and the rocker-frame connection.
- The links should not be too short or too long, as shorter links would lead congestion in the mechanism, while longer links would add weight, thus increasing required motor power. Therefore, 15 cm and 50 cm were kept as the lower and upper limit of the link lengths, respectively.

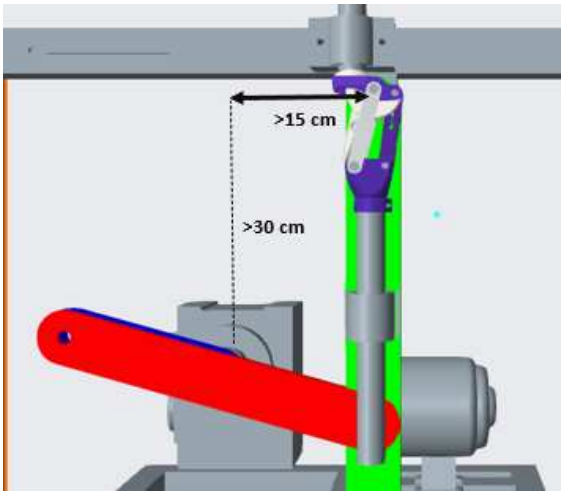

Figure 2.5: Constraints based on the motor position

2.2.3 Link Lengths Optimization

The designed mechanism should be compact. One way of achieving that is aiming to minimise the area swept by the mechanism while satisfying the given conditions. Therefore, the maximum rectangular area swept by the mechanism during its one complete cycle of motion was taken to be the minimization function.

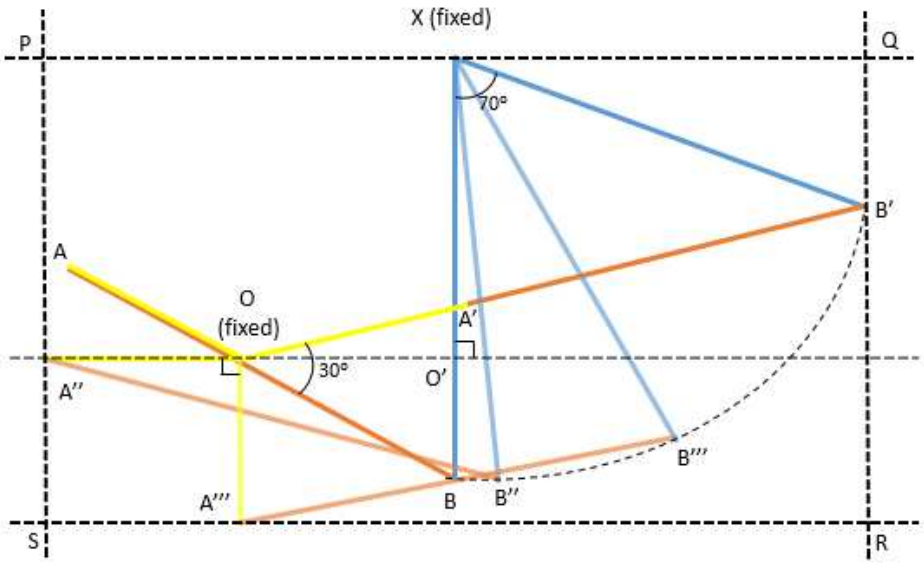

Figure 2.6: The maximum rectangular area swept by the mechanism during one complete cycle is represented by PQRS, which is to be minimised.

The rectangular area swept will be (horizontal sweep) $*$ (vertical sweep)

Horizontal Sweep: The maximum horizontal sweep = length of crank + horizontal distance between the motor-crank connection and the rocker-frame connection + horizontal projection of rocker at the extreme position.

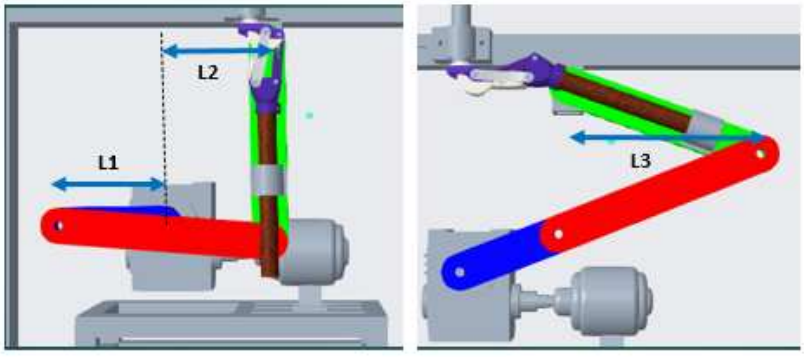

Figure 2.7: Horizontal Sweep

$$\textit{Horizontal sweep} = L1 + L2 + L3$$
$$= PQ = A''O + OO' + XB' * sin(70)$$

Vertical Sweep: The maximum vertical sweep = **Max** (length of the rocker, the vertical distance between the motor-crank connection and the rocker-frame connection + length of the crank)

$$\textit{Vertical sweep} = QR = max(XB, XO' + OA''')$$

The equations and constraints described above were added in the MATLAB code. It was run by varying 'H' from 30 cm to 45 cm in steps of 0.1 cm and varying 'α' from -60^o to 60^o in steps of 1^o. A very high value of the rectangular area was initialized, and as smaller values were subsequently obtained, they were stored. The optimal solution was obtained at H = 300 and $\alpha = -7^o$. The obtained optimal link lengths were:

- Crank = **16.852 cm**
- Connecting rod = **32.046 cm**
- Rocker = **31.851 cm**
- Base = **33.577 cm** (base i.e. the distance between crank-motor connection and rocker-frame connection)

But, it is difficult to manufacture links of the above calculated lengths. So, the link lengths were slightly modified, while ensuring that the constraints considered earlier are largely met. Finally, the **lengths of the crank, connecting rod and rocker were taken to be 17 cm, 35 cm and 33 cm, respectively.**

Table 2.1: Comparison of the four-bar linkage parameters between the initially calculated and finally considered values.

Item	Calculated	Actual
Crank	16.852 cm	17 cm
Coupler	32.046 cm	35 cm
Rocker	31.851 cm	33 cm
Hor. Sweep	61.86 cm	65.3 cm
Ver. Sweep	46.85 cm	51.5 cm
Rect. area	2898.14 cm^2	3362.95 cm^2

CHAPTER 3

FORCE AND MOTION ANALYSIS

Once the link lengths were finalized, the forces and torques acting at various points of the system were calculated. Based on these values, various parameters of the design were determined , such as motor specifications, material and thickness of links, frames, etc. The formulations were initially done in MATLAB, and the results were ascertained by simulations done in ADAMS. The MATLAB code for the analysis can be found in Appendix 2.

3.1 Kinematic Analysis

First, the kinematics of the system was analysed, and using those values, the forces and torques were calculated.

Taking A as the origin $\Rightarrow A = [0, 0]$

$D = [AD, 0]$

$B = [AB * cos(\delta), AB * sin(\delta)]$

$\overrightarrow{BD} = \overrightarrow{DA} + \overrightarrow{AB}$

$|BD|^2 = |DA|^2 + |AB|^2 +$

$$2 * |DA| * |AB| * cos(\theta)$$

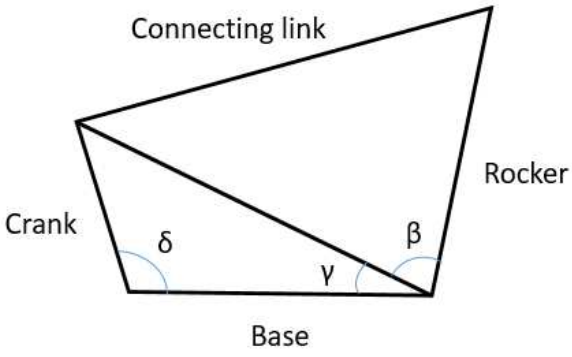

Figure 3.1: Fourbar linkage

Using Cosine Rule,

$$cos(\gamma) = \frac{BD^2 + AD^2 - AB^2}{2 * BD * AD}$$

$$cos(\beta) = \frac{BD^2 + CD^2 - CB^2}{2 * BD * CD}$$

Thus,

$C = [AD - CD * cos(\gamma + \beta), CD * sin(\gamma + \beta)]$

Once $\delta(t)$ is known, the above equations can be used to find the positions of the vertices B and C.

The velocities at those points can be found by:

$$(V_X)_B = \frac{d(X)_B}{dt} \qquad (V_Y)_B = \frac{d(Y)_B}{dt}$$
$$(V_X)_C = \frac{d(X)_C}{dt} \qquad (V_Y)_C = \frac{d(Y)_C}{dt}$$

Similarly, the accelerations at those points can be found by:

$$(a_X)_B = \frac{d(V_X)_B}{dt} \qquad (a_Y)_B = \frac{d(V_Y)_B}{dt}$$
$$(a_X)_C = \frac{d(V_X)_C}{dt} \qquad (a_Y)_C = \frac{d(V_Y)_C}{dt}$$

Since the links will be very similar in shape as rods, the velocities and accelerations of the centre of mass of each of the links could be taken to be the average of the velocities and accelerations of both ends.

$$(V_X)_{crank} = \frac{(V_X)_B}{2} \qquad (V_Y)_{crank} = \frac{(V_Y)_B}{2}$$
$$(V_X)_{coupler} = \frac{(V_X)_B + (V_X)_C}{2} \qquad (V_Y)_{coupler} = \frac{(V_Y)_B + (V_Y)_C}{2}$$
$$(V_X)_{rocker} = \frac{(V_X)_C}{2} \qquad (V_Y)_{rocker} = \frac{(V_Y)_C}{2}$$

$$(a_X)_{crank} = \frac{(a_X)_B}{2} \qquad (a_Y)_{crank} = \frac{(a_Y)_B}{2}$$
$$(a_X)_{coupler} = \frac{(a_X)_B + (a_X)_C}{2} \qquad (a_Y)_{coupler} = \frac{(a_Y)_B + (a_Y)_C}{2}$$
$$(a_X)_{rocker} = \frac{(a_X)_C}{2} \qquad (a_Y)_{rocker} = \frac{(a_Y)_C}{2}$$

The angular velocities of the crank, coupler and the rocker links can be calculated as:

- $\omega_{crank} = \dfrac{d\delta(t)}{dt}$
  In this case, this will be a constant as the crank is rotated at a constant angular velocity.
- $\omega_{coupler} = \dfrac{(V_Y)_C - (V_Y)_B}{(X)_C - (X)_B}$
- $\omega_{rocker} = \dfrac{-(V_X)_C}{(Y)_C}$

The angular accelerations of the links will be:

- $\alpha_{crank} = 0$, as crank is rotated with constant angular velocity.
- $\alpha_{coupler} = \dfrac{d\omega_{coupler}}{dt}$
- $\alpha_{rocker} = \dfrac{d\omega_{rocker}}{dt}$

The average cadence is 100 - 115 steps/min for adult humans. Thus, for each leg, the number of steps is 50-58/min. That implies each leg undergoes 50-58 swing phases per minute. But since the swing phase only accounts for about 40% of a gait cycle, the effective number of swing phases per minute would be 125-145. For prosthesis users, this number would be quite lower, and an upper limit of 120 could be considered. Since in this mechanism, stance phase is not taken into account while testing and instead, the knee joint is put in a continuously swinging mode, this should be the speed (in rpm) at which the motor runs.

Thus, running the mechanism at 120 rpm, the following results are obtained:

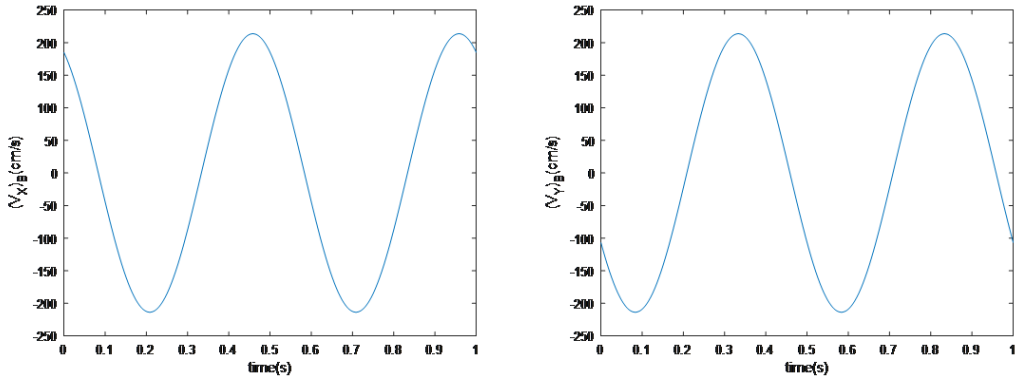

Figure 3.2: Velocity components of free end of crank

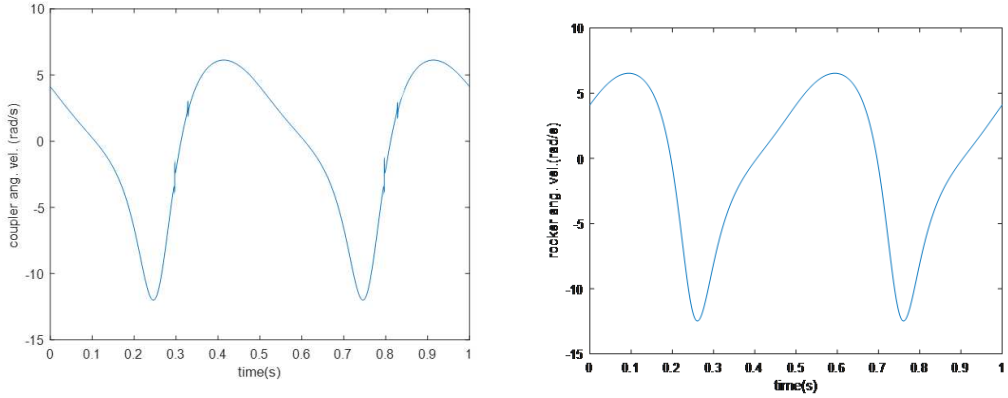

Figure 3.4: Angular velocity of coupler and rocker

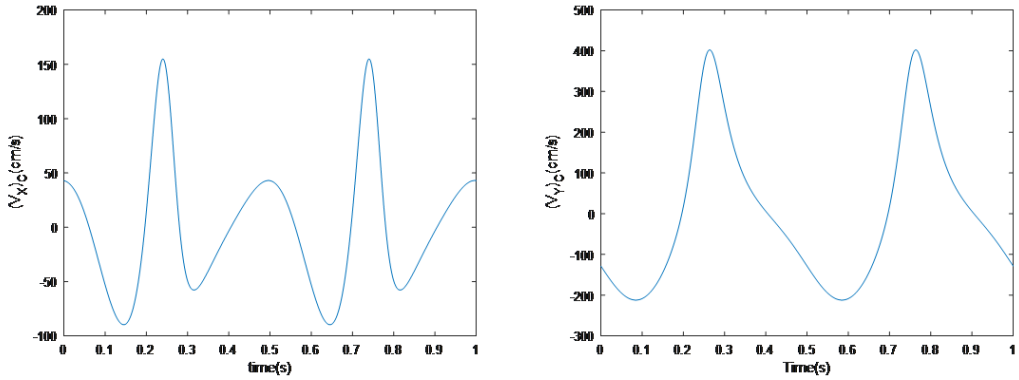

Figure 3.3: Velocity components of free end of rocker

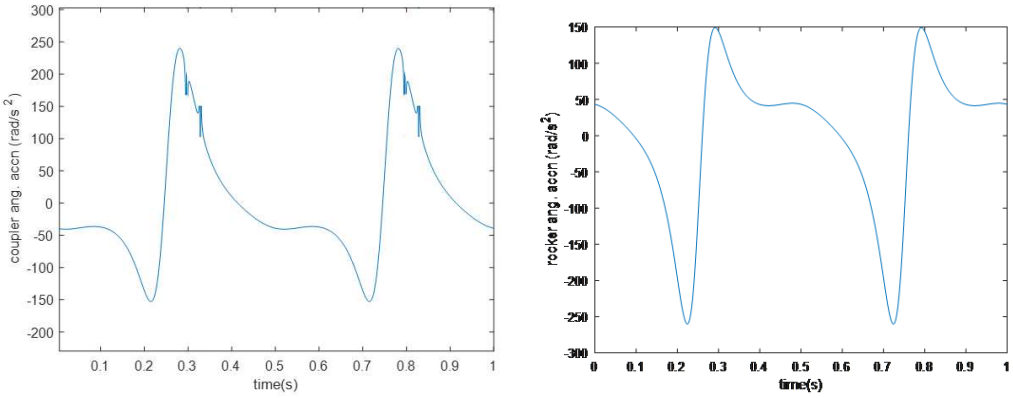

Figure 3.5: Angular velocity of coupler and rocker

3.2 Dynamic Analysis

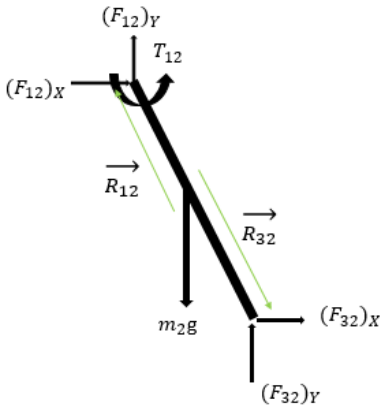

$$(F_{12})_X + (F_{32})_X = m_2 a_{Gx_2};$$
$$(F_{12})_Y + (F_{32})_Y - m_2 g = m_2 a_{Gy_2};$$
$$T_{12} + [(F_{12})_Y R_{12_X} - (F_{12})_X R_{12_Y}] + [(F_{32})_Y R_{32_X} - (F_{32})_X R_{32_Y}] = I_{G_2}\alpha_2;$$

Figure 3.6: FBD of Crank

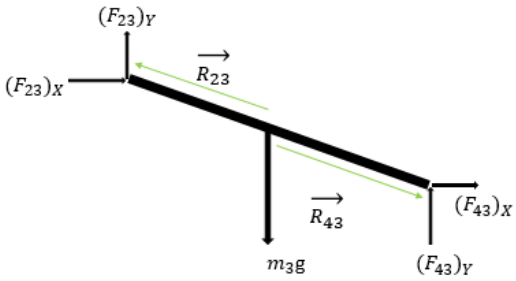

$$F_{23} = -F_{32};$$
$$(F_{23})_X + (F_{43})_X = m_3 a_{Gx_3};$$
$$(F_{23})_Y + (F_{43})_Y - m_3 g = m_3 a_{Gy_3};$$
$$[(F_{23})_Y R_{23_X} - (F_{23})_X R_{23_Y}] + [(F_{43})_Y R_{43_X} - (F_{43})_X R_{43_Y}] = I_{G_3}\alpha_3;$$

Figure 3.7: FBD of Coupler

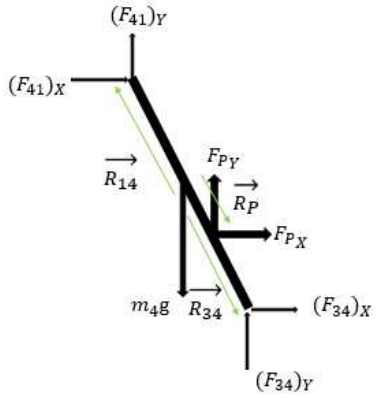

$$F_{34} = -F_{43};$$
$$(F_{14})_X + (F_{34})_X + (F_P)_X = m_4 a_{Gx_4};$$
$$(F_{14})_Y + (F_{34})_Y + (F_P)_Y - m_4 g = m_4 a_{Gy_4};$$
$$[(F_{14})_Y R_{14_X} - (F_{14})_X R_{14_Y}] + [(F_{34})_Y R_{34_X} - (F_{34})_X R_{34_Y}] + (F_{P_Y} R_{P_X} - F_{P_X} R_{P_Y}) = I_{G_4}\alpha_4;$$

Figure 3.8: FBD of Rocker

F_P is the force transferred to the rocker at the point of connection of the shank to the rocker. It includes the force due to the mass of the shank and foot (6.43% of body weight[23]) and the force necessary to rotate the shank along with the rocker.

Putting all the above equations in a matrix, we obtain:

$$\begin{bmatrix} 1 & 0 & 1 & 0 & 0 & 0 & 0 & 0 & 0 \\ 0 & 1 & 0 & 1 & 0 & 0 & 0 & 0 & 0 \\ -R_{12_Y} & R_{12_X} & -R_{32_Y} & R_{32_X} & 0 & 0 & 0 & 0 & 1 \\ 0 & 0 & -1 & 0 & 1 & 0 & 0 & 0 & 0 \\ 0 & 0 & 0 & -1 & 0 & 1 & 0 & 0 & 0 \\ 0 & 0 & R_{23_Y} & -R_{23_X} & -R_{43_Y} & R_{43_X} & 0 & 0 & 0 \\ 0 & 0 & 0 & 0 & -1 & 0 & 1 & 0 & 0 \\ 0 & 0 & 0 & 0 & 0 & -1 & 0 & 1 & 0 \\ 0 & 0 & 0 & 0 & R_{34_Y} & -R_{34_X} & -R_{14_Y} & R_{14_X} & 0 \end{bmatrix} * \begin{bmatrix} (F_{12})_X \\ (F_{12})_Y \\ (F_{32})_X \\ (F_{32})_Y \\ (F_{43})_X \\ (F_{43})_Y \\ (F_{14})_X \\ (F_{14})_Y \\ T_{12} \end{bmatrix}$$

$$= \begin{bmatrix} m_2 a_{Gx_2} \\ m_2 a_{Gy_2} + m_2 g \\ I_{G_2} \alpha_2 \\ m_3 a_{Gx_3} \\ m_3 a_{Gy_3} + m_3 g \\ I_{G_3} \alpha_3 \\ m_4 a_{Gx_4} - F_{P_X} \\ m_2 a_{Gx_2} - F_{P_Y} + m_4 g \\ I_{G_4} \alpha_4 - F_{P_Y} R_{P_X} + F_{P_X} R_{P_Y} \end{bmatrix}$$

Inverting the first matrix and multiplying on both sides, we will get the matrix containing the values of the forces and torques $((F_{12})_X, (F_{12})_Y, \ldots T_{12})$. These values are dependent on accelerations and angular accelerations, which were calculated previously. All these values vary with the configuration of the system at that time, and thus a code was written to calculate and store these values over the complete cycle.

3.3 Links material and thickness

Various materials were considered for links like steel, aluminium, carbon fibres, etc. The forces and torques were calculated and tested for safety by performing FEA in ANSYS. The thickness of the links was decided such that the weight of the links should not be too high, but should also be able to sustain the forces acted on them during the cycle. Alongside, other factors like cost and availability, machinability, etc., were considered, and finally, 10 mm thickness of EN8 steel was considered the best for our links.

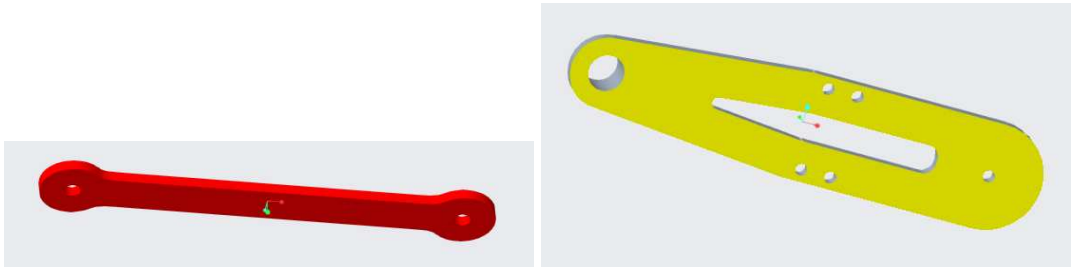

Figure 3.9: Updated designs of links: Crank (L) and Rocker (R)

The crank and coupler links were reduced in width in the middle to reduce their mass and moments of inertia. Also, the rocker width was increased to accommodate the joint with the shank pylon. To compensate for the increase in mass, material from the middle of the link was removed.

As a conservative approach, while performing the finite element analysis in ANSYS, the maximum forces at each joint for a complete cycle was considered.

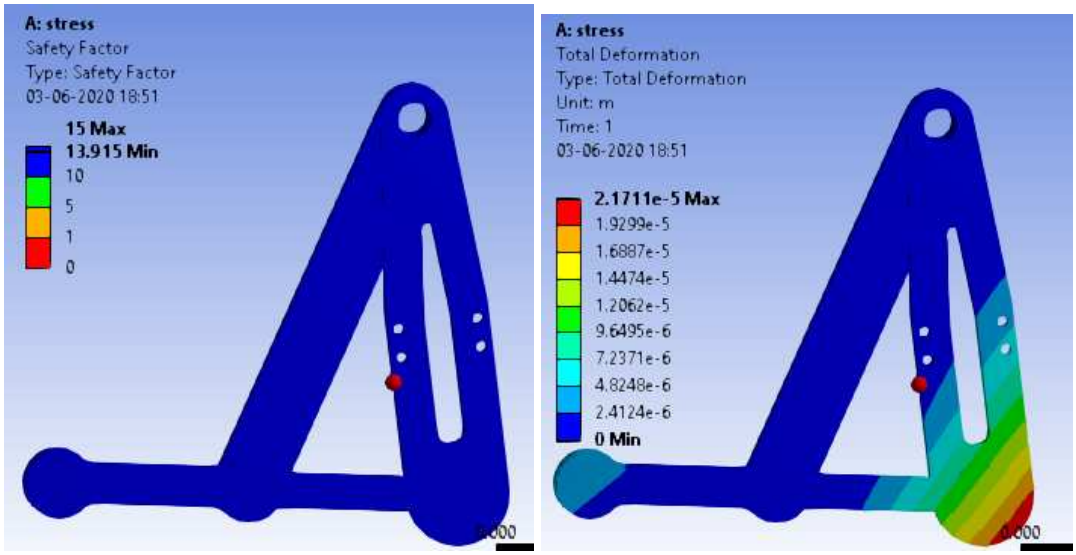

Figure 3.10: Total deformation and safety factor for steel links

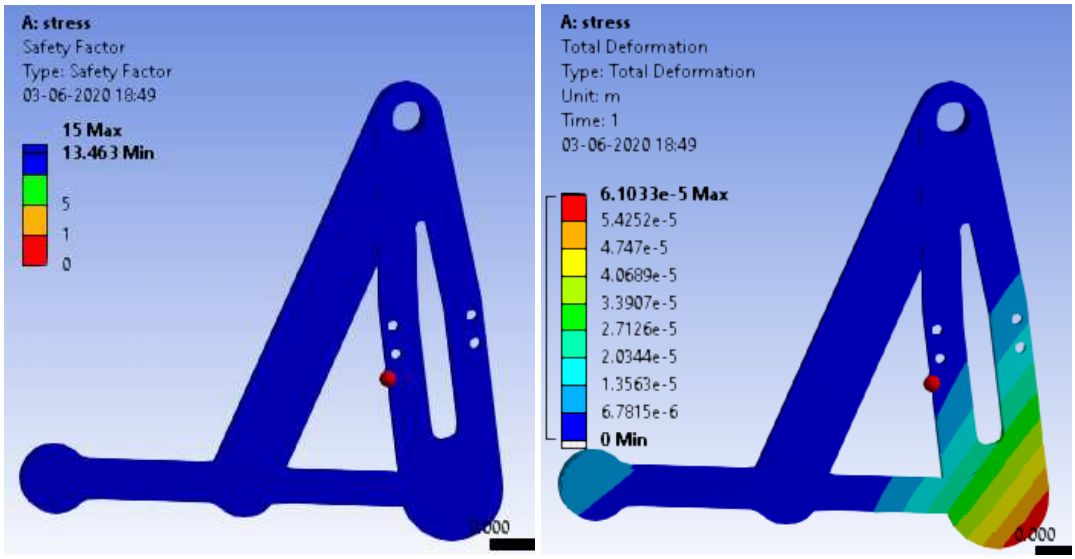

Figure 3.11: Total deformation and safety factor for Aluminum alloy links

3.4 Motor and Gearbox Selection

Based on the required torque to rotate the system at 120 rpm, the motor specifications are decided.

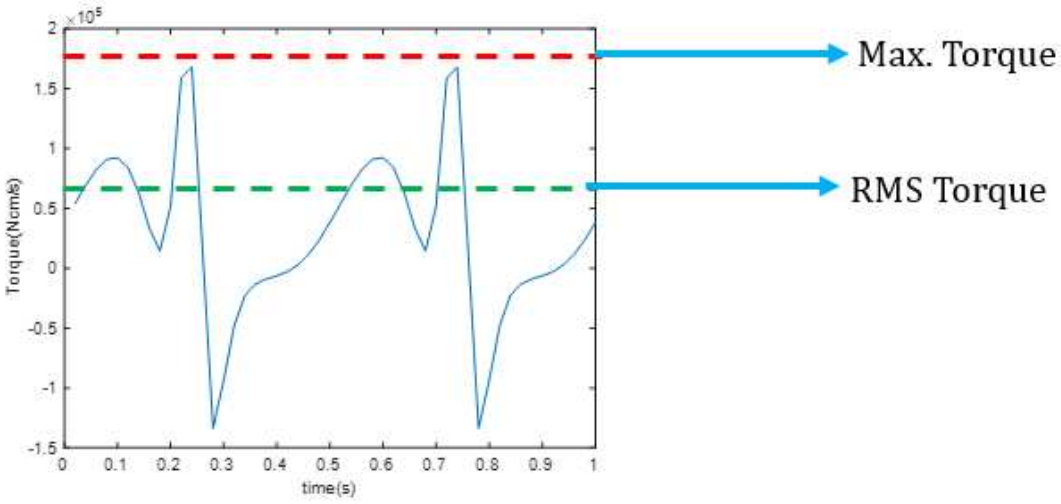

Figure 3.12: Torque variation over two complete cycles

$$\text{RMS Torque} = \sqrt{\frac{\sum {torque_i}^2 * time_i}{\sum time_i}} = 7.277Nm$$

$$\text{Maximum Torque} = 16.804Nm$$

In the case of our mechanism, the load is variable. Thus,it should be ensured that:

1. Peak Load Power $<$ Rated Motor Power $* \dfrac{1 + \text{Service factor in \%}}{100}$
2. The RMS Load Power must be less than the Rated Motor Power.

For this mechanism,

$$\text{Peak Load Power requirement} = \frac{T_{max} * N * 2 * \pi}{60} = \frac{16.804 * 120 * 2 * \pi}{60} = 211.16W$$

$$\text{RMS Load Power requirement} = \frac{T_{rms} * N * 2 * \pi}{60} = \frac{7.277 * 120 * 2 * \pi}{60} = 91.45W$$

- Assuming an efficiency of 75% due to frictional losses,

  $$\text{Peak Motor power} = \frac{211.16 * 100}{75} = 281.55W$$

  $$\text{RMS Motor Power} = \frac{91.45 * 100}{75} = 121.93W$$

- Generally, the Service factor of induction motors is 10%. So, a motor with a rated power of $\dfrac{281.55}{1.1}$ = 255.95 W or above should be sufficient. A motor

with a rated power of 0.5 HP or 372.85 W was available, which can be used for the mechanism

GEARBOX: Generally, motors available in the required power range have a rated speed of 1200-1400 rpm. Thus, a gearbox is required to reduce the speed. The gearbox should have an effective gear ratio of ~ 10.A gearbox with a gear ratio of 10 was available, which can be considered for the mechanism.

3.5 Frame design

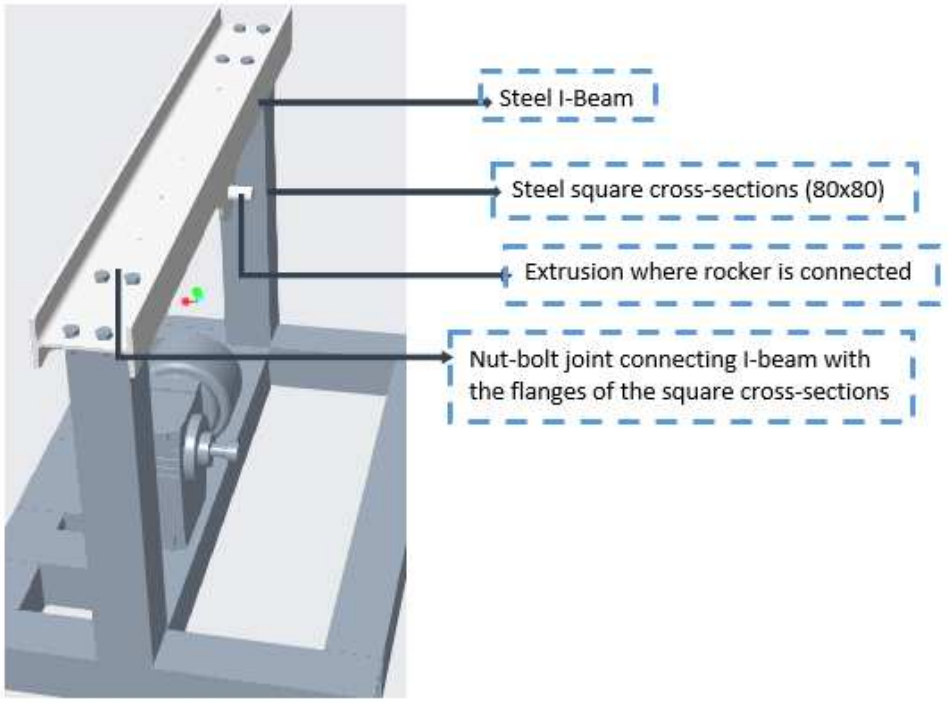

Figure 3.13: Design of the frame

The designed frame includes a mild steel I-beam of 1m length on top and 80x80 steel square cross-sections for support and base. The height and the end-to-end separation of the vertical columns are taken to be 63.5 cm and 82 cm, respectively, using the rectangular area calculations done during link length optimization into perspective. These columns are welded to flanges at one end, which provides a surface for nut-bolt joints with the beam. A wide base is designed to provide support, as well as to lower the center of mass of the system, thus improving stability. The base is designed to be 60 cm wide, with 30 cm lying in front of the vertical channels, and 22 cm at the rear.

Smaller sections are attached in the rear-side of the base for proper placement of the motor-gearbox system.

One end of the rocker is connected to the frame at the point shown in Fig 3.13. At this joint, the reaction forces are considerably high. Figure 3.14 shows the plot of the reaction force components acting at that joint. It is necessary to ascertain the safety of the components which are directly affected by these forces.

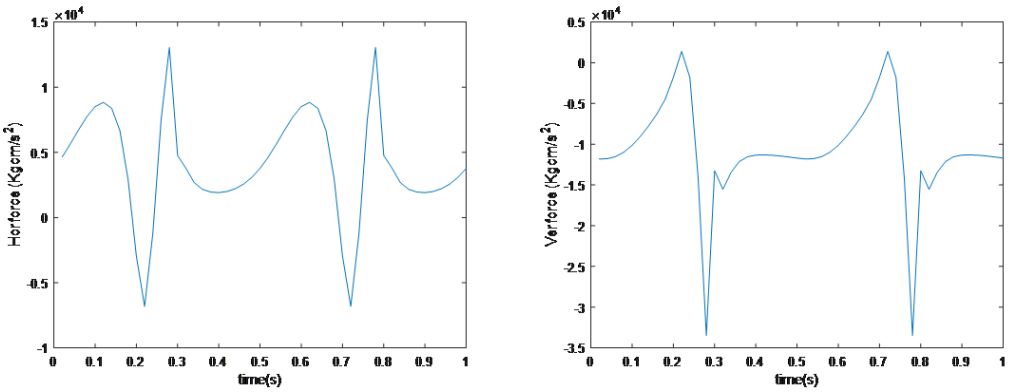

Figure 3.14: Plots of horizontal and vertical frame forces over two complete cycles

The I-beam's web acts as a base on which the linear guide system is installed. A standard dimension (125x70) I-beam is considered, which is sufficient to accommodate the linear guide system on it. A flange is welded to one of the outermost edges of the I-beam, which in turn is welded to a small rod which will support the rocker. The design of that rod needs to be looked into. As the beam is selected to be made of mild steel, this rod has also been chosen to be made out of MS.

$$r = 11mm$$

$$I = \frac{\pi r^4}{4} = 1.1510^8 m^4$$

$$F_{max} = 375N$$

$$M_{max} = F_{max} * 0.03m = 11.25Nm$$

$$\sigma = \frac{M_{max} y}{I} = 10.7MPa$$

$$\text{Factor of safety} = \frac{\sigma_y}{\sigma} = 23.2$$

Stainless steel square cross-sectioned hollow channels were chosen to be used as

the material for support and base because they provide a good moment of inertia with lower weight and provide sufficient surface for fixing studs or bolts.

A major failure concern with the truss members is buckling of the compression members. In this mechanism, the vertical sections experience the maximum compressive forces, because of the combined load due to the reaction force and the I-beam's weight, and thus their safety against buckling was ascertained.

Steel channel of outer square size 80 mm and material thickness 4.5 mm was available, and hence calculations were done assuming those dimensions. The moment of

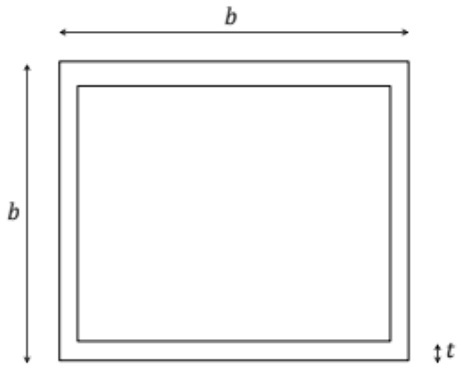

Figure 3.15: Illustration of the square cross-section

inertia for the box channel is given by:

$$I = \frac{1}{6}bt^3 + \frac{1}{2}bt(b-t)^2 + \frac{1}{6}t(b-2t)^3$$

Putting b as 80 mm and t as 4.5 mm,

$$I = 1.296 * 10^{-6} m^4$$

According to the Euler Buckling formula, the critical buckling force for a fixed-free column is given by:

$$P_{cr} = \frac{\pi^2 E_{SS} I}{L_{eff}^2} = 2300KN.$$

Taking $E_{SS} = 180$ GPa and $L_{eff} = 2l$ for a fixed-free column, the obtained critical buckling force was 575KN and the factor of safety (FoS) was ≈ 1000.

Although 1000 seems like an over design, we would continue with the same SS

channel. The channels are supporting an I-beam of 125 mm width, and thus need to be sufficiently wide for apt connection. Also, for the frame, a total length of 4.8 m channel is required. Since the minimum standard available length is 6 m, using a channel of the same dimensions everywhere reduces wastage of materials. Finally, a finite element stress analysis of the frame was carried out with appropriate loads in ANSYS

To avoid vibrations while the mechanism is in action, the frame could be fixed at few positions to the ground with ground pins.

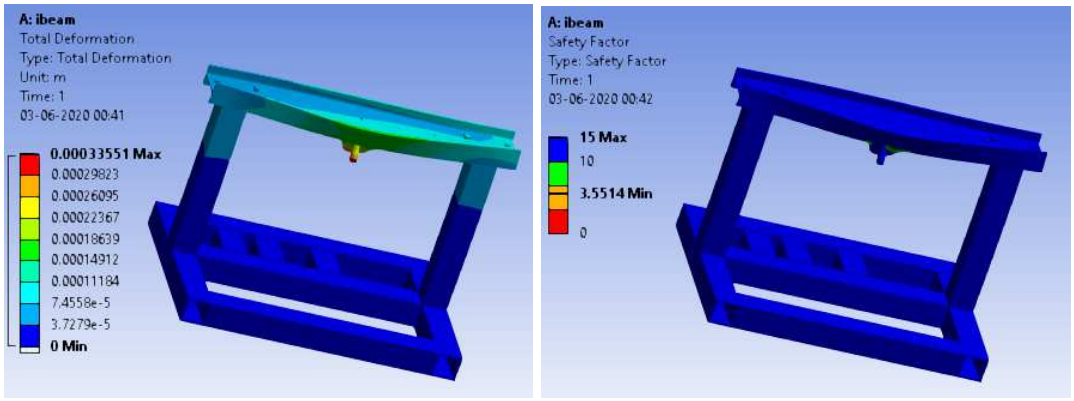

Figure 3.16: The deformation and factor of safety for the designed frame. The maximum deformation was observed to be 0.33 mm

CHAPTER 4

SELECTION OF INDUSTRIAL COMPONENTS

4.1 Bearings

We have 3 locations where we need to use bearings, at the crank-coupler, coupler-rocker and rocker-frame joint. We used AGMA standard equations to determine the bearings for our model[24].

The dynamic load-carrying capacity of a bearing is defined as the load that can be carried for a minimum life of one million revolutions (L_{10}):

$$L_{10} = (\frac{C}{P})^N$$

Where, L_{10}=rated bearing life in million revolutions with 90% reliability

C= dynamic load-carrying capacity (N)

P= equivalent bearing load (N)

N= 3 for ball bearings, N= $\frac{10}{3}$ for roller bearings

P = Equivalent Bearing load (N) = $XVF_r + YF_a$

Where, F_r= radial load in (N)

F_a= thrust load in (N)

V = rotation factor, V = 1 if inner race rotates

V = 1.2 if outer race rotates

'X' and 'Y' are dependent on the ratio of radial and axial load. For cases of no axial loads, as in here, X = 1 and Y =0.

Table 4.1: Maximum load at joints

Joint with bearing	Maximum Load (N)
Crank-Coupler	170.3
Coupler-Rocker	186.35
Rocker-Frame	366.75

The C_{10} load rating of the bearings is 5.1KN. Thus, the life of the bearings:

- At crank-coupler joint = $(\frac{5100}{170.3})^3$=26857 million cycles at 90% reliability

  = $(\frac{5100}{1.2 * 170.3})^3 * (0.02 + 4.439 * (0.01)^{\frac{1}{1.483}}))$

  = 3402 million cycles at 99% reliability

- At coupler-rocker joint = $(\frac{5100}{186.35})^3$=20498 million cycles at 90% reliability

  = $(\frac{5100}{1.2 * 186.35})^3 * (0.02 + 4.439 * (0.01)^{\frac{1}{1.483}}))$

  = 2596 million cycles at 99% reliability

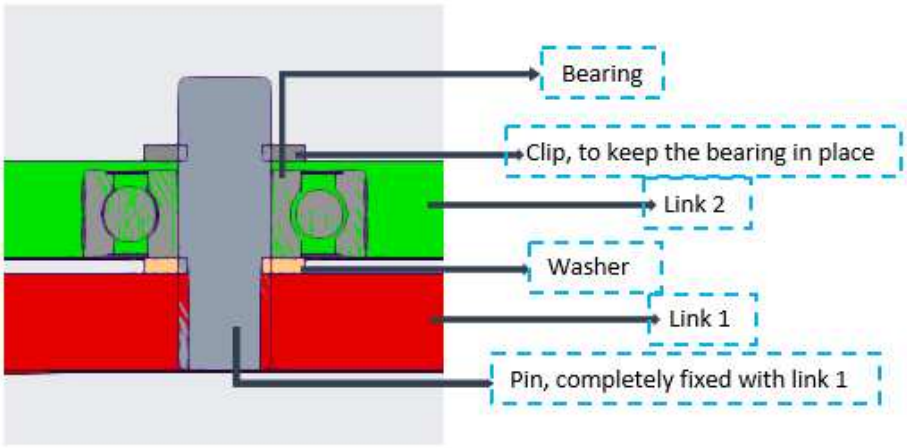

Figure 4.1: Sectional cross-section of crank-coupler joint

For connection at the rocker-frame joint, we have selected Single-Row Solid Needle roller bearing with a bore diameter of 22 mm and an outer diameter of 30 mm and 20 mm width (Part no.: NK22/20R). We have selected roller bearing here to spread the load over a larger area at the joint for the safety of the extrusion.

The C_{10} load rating of the bearings is 18 KN. Thus, using similar methods as above, the life of the roller bearing = 1483 million cycles at 99% reliability

4.2 Bushing

The standard pylon tubes are 30 mm in diameter. Thus, we selected a bushing that has a bore diameter of 30 mm.

Table 4.2: Parameters of the selected bushing

Model No.	Weight (g)	Shaft dia. (mm)	Length (mm)	Width (mm)
SC30UU	555	30	72	78

4.3 Linear Guide System

For our mechanism, we have selected a linear guide system with the following specifications:

- Rated $F_y = 20.1KN$
- Rated $F_z = 24.8KN$
- Rated $M_x = 0.44KNm$
- Rated $M_y = 0.352KNm$
- Rated $M_y = 0.352KNm$

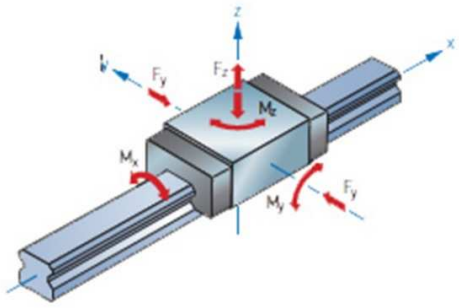

Figure 4.2: Forces and moments on linear guides[3]

Although the actual forces and moments acting on the guide are considerably lesser than the rated values, we have considered a higher-rated guide, taking into account the very long running time and subjection to sudden jerks while running.

The linear rail was taken to be of 520 mm long.

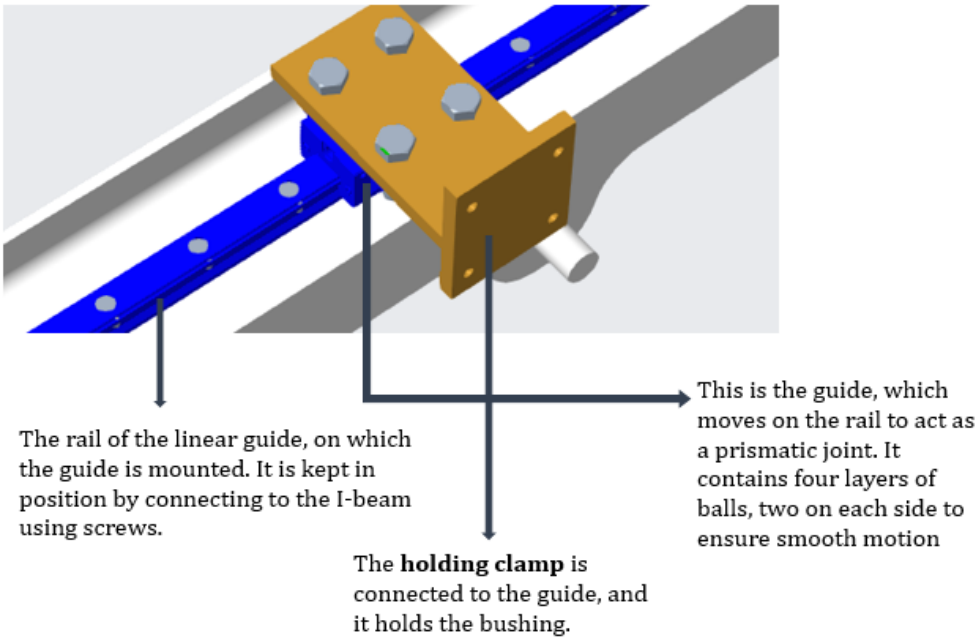

Figure 4.3: Linear Guide assembly

CHAPTER 5

CONCLUSION

This work resulted in the ideation and development of a new technique for testing the walking longevity of prosthetic knee joints by using a four-bar mechanism as a simulator for the swing phase of a walking gait cycle.

This design provides a standard method for testing of both polycentric and single-axis knees of various sizes. Without human interference, the mechanism can run continuously to determine the number of cycles the knees will last, and thus the distance for which they could be used safely. A universal mechanism was worked out that could fit a variety of prosthetic knee systems by investigating their mechanisms in detail. A compact stationary setup to install the mechanism was designed as well. Overall this work paves the way towards the development of a standard procedure to determine the longevity of prosthetic knee joints.

Future work would involve the manufacturing of the setup and testing available prosthetic knees to assess their life. Since this mechanism functions as a testing medium for only the swing phase of the gait cycle, modification of this technique to accommodate testing of the stance phase could be looked into, thus integrating both the phases to test the knees for the complete gait cycle using a single mechanism.

APPENDIX A

Manufacturing Drawings

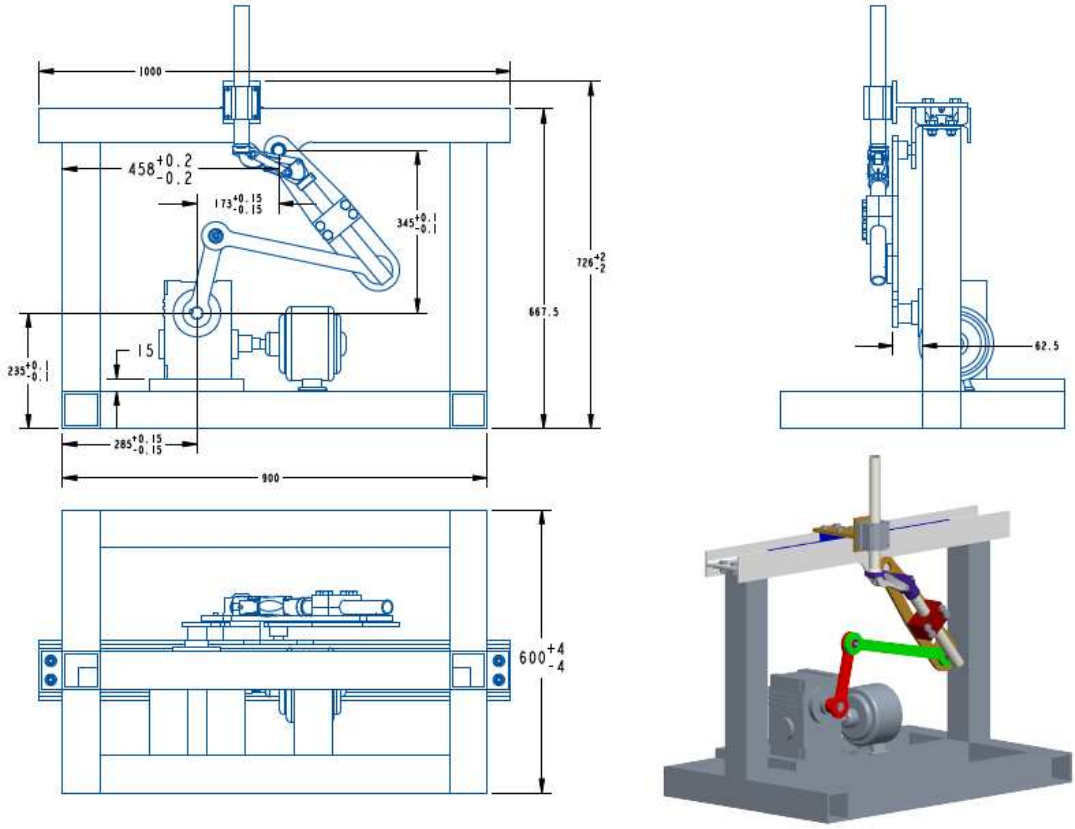

Figure A.1: Complete Model: Dimensions and tolerances

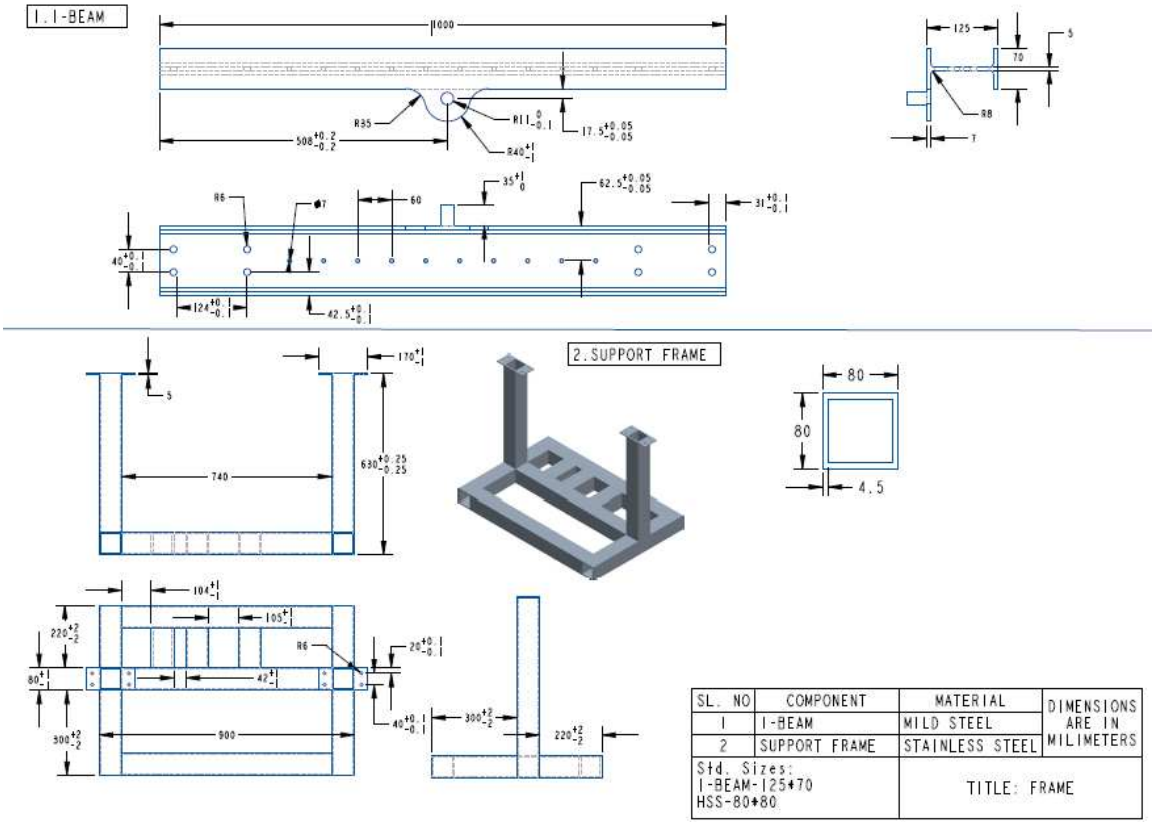

Figure A.2: Frames: Dimensions and tolerances

Table A.1: Frame Components

Item	Length (mm)	Number
I-Beam (125x70)	1000	1
Hollow Cross-Section (80x80)	625	2
Hollow Cross-Section (80x80)	740	3
Hollow Cross-Section (80x80)	300	2
Hollow Cross-Section (80x80)	220	2
Hollow Cross-Section (80x80)	140	3

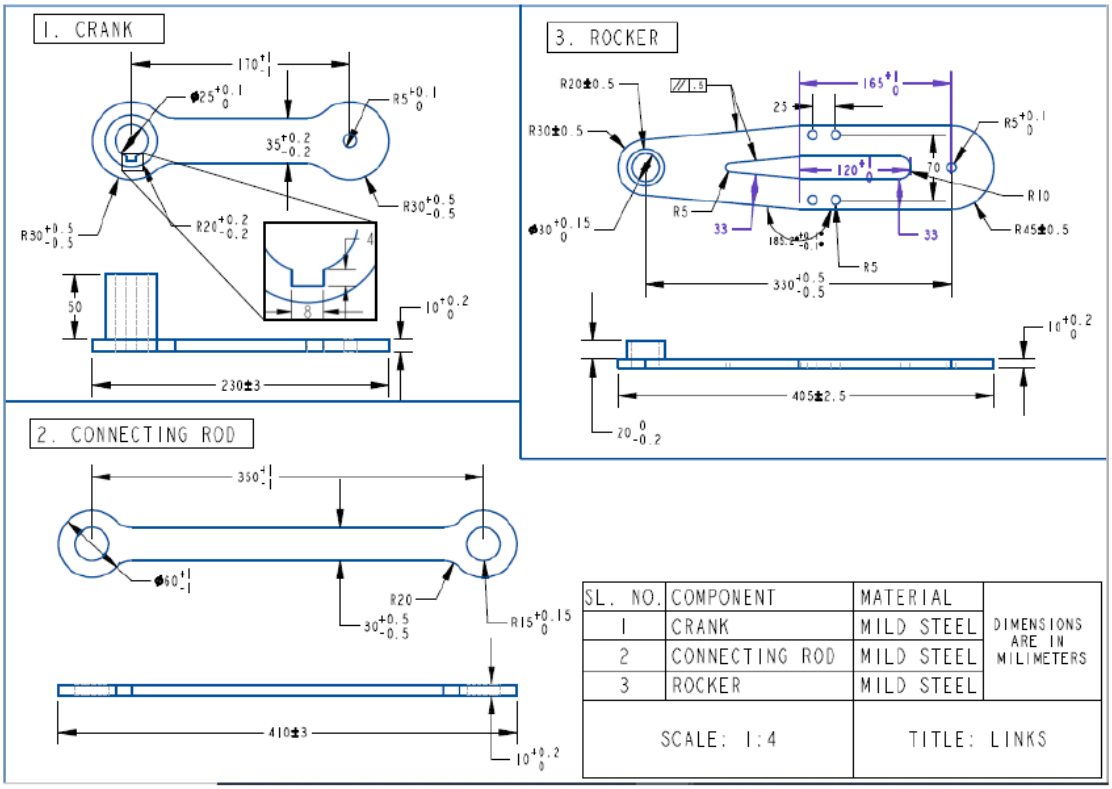

Figure A.3: Links: Dimensions and tolerances

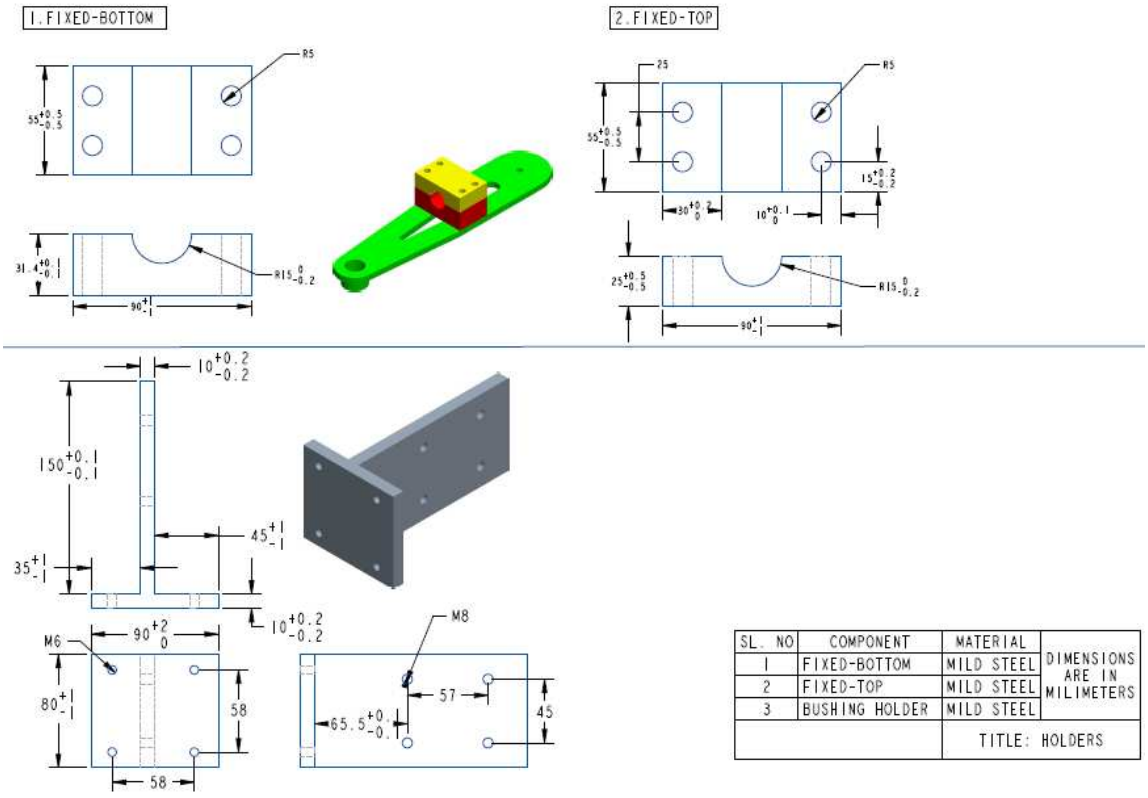

Figure A.4: Holders: Dimensions and tolerances

APPENDIX B

Code for link lengths optimization

```
opt=1000000; %initial high value
opt_m= 1000000*ones(1,151);
index= zeros(1,151);
for H=300:1:450 %loop with changing the vertical distance betn frame
    connections of crank and rocker
for t=-60:1:60  %loop with changing the starting angle
    alpha=t*pi/180;
    Coeff =[sin(alpha) 0 1 0;0 cos(alpha+(30*pi/180)) -sin(70*pi/180)
     -1;...
        cos(alpha) 0 0 -1;0 sin(alpha+(30*pi/180)) cos(70*pi/180) 0];
    RHS = [H;0;0;H];
    Len=inv(Coeff)*RHS;
    L(t+61,1)=Len(1);%min position(connecting rod-crank)
    L(t+61,2)=Len(2);%max position(crank+connecting rod)
    L(t+61,3)=Len(3);%rocker
    L(t+61,4)=Len(4);%hor_distance betn frame connections of crank
    and rocker
    link(t+61,1)=0.5*(Len(2)-Len(1));%crank
    link(t+61,2)=0.5*(Len(2)+Len(1));%connecting rod
    link(t+61,3)=Len(3);%rocker
    link(t+61,4)=sqrt(H^2+Len(4)^2);%fixed support

    max_ver = max(H+link(t+61,1),link(t+61,3));%max ver
    max_hor = link(t+61,1)+L(t+61,4)+link(t+61,3)*sin(70*pi/180);%max
     hor. coverage
    rect_area = (max_ver*max_hor);

    Condn =[link(t+61,1)>150;link(t+61,2)>150;link(t+61,3)>150;...
        link(t+61,1)<500;link(t+61,1)<500;link(t+61,1)<500;...
        L(t+61,4)>150;link(t+61,1)<link(t+61,2);link(t+61,1)<link(t
    +61,3);...
        link(t+61,1)<link(t+61,4);2*(max(link(t+61,:))+min(link(t
    +61,:)))<sum(link(t+61,:))];%constraints matrix
```

```
28      if Condn == [1;1;1;1;1;1;1;1;1;1;1;1] %boolean matrix to satisfy
    constraints
29          if rect_area < opt %if a better solution is found, it is
    stored.
30              opt = rect_area;
31              opt_m(H-299)=opt;
32              index(H-299) = t+61;
33              Hor_size = max_hor;
34              Ver_size = max_ver;
35              Angle = alpha*180/pi;
36              Height = H;
37              Links = [link(t+61,1) link(t+61,2) link(t+61,3) link(t
    +61,4)];
38          end
39      end
40  end
41  end
42  %%type 'Links' in command window to get the link lengths
43  %%type 'Angle' and 'Height' to get the parameters 'alpha' and 'H' for
        these link lengths
```

APPENDIX C

Code for Kinematic and Dynamic analysis

```
clc; clear all;
A = 17;B=35;C=33;D=35; % Link lengths in cm

t = 0:0.02:3;

ang_speed = 4*pi; %crank angular vel.
theta = ang_speed*t;
%% POSITIONS AND VELOCITIES
P1 = [0;0];
P4 = D*[-1;0];%P1 and P4 are fixed points

P2 = A*[cos(theta); sin(theta)];%P2 is non-fixed end of crank
P2_x = P2(1,:);
P2_y = P2(2,:);

P2_vx = diff(P2_x)./diff(t);
P2_vy = diff(P2_y)./diff(t);

A_CG_x = P2(1,:)/2;% posn. and vel. of COM of crank
A_CG_y = P2(2,:)/2;
A_CG_vx = diff(A_CG_x)./diff(t);
A_CG_vy = diff(A_CG_y)./diff(t);

E = sqrt(A^2 + D^2 + 2*A*D*cos(theta));
alfa = asin(A*sin(theta)./E);
beta = acos((E.^2 + C^2 - B^2)./(2*E*C));
P3 = [-D + C*cos(alfa+beta); C*sin(alfa+beta)];%P3 is non-fixed end
    of rocker

P3_x = P3(1,:);
P3_y = P3(2,:);

P3_vx = diff(P3_x)./diff(t);
P3_vy = diff(P3_y)./diff(t);
```

```
34
35 P3_v = sqrt(P3_vx.^2 + P3_vy.^2);
36
37 B_CG_x = (P2(1,:)+P3(1,:))/2;%posn. and vel. of COM of coupler
38 B_CG_y = (P2(2,:)+P3(2,:))/2;
39 B_CG_vx = diff(B_CG_x)./diff(t);
40 B_CG_vy = diff(B_CG_y)./diff(t);
41
42 C_CG_x = (P3(1,:)-D)/2;%posn. and vel. of COM of rocker
43 C_CG_y = P3(2,:)/2;
44 C_CG_vx = diff(C_CG_x)./diff(t);
45 C_CG_vy = diff(C_CG_y)./diff(t);
46
47 %% ACCELERATIONS
48 t = 0.02:0.02:3;
49 A_CG_ax = diff(A_CG_vx)./diff(t);%accn of COM of crank
50 A_CG_ay = diff(A_CG_vy)./diff(t);
51 A_CG_a = sqrt(A_CG_ax.^2 + A_CG_ay.^2);
52 B_CG_ax = diff(B_CG_vx)./diff(t);%accn of COM of coupler
53 B_CG_ay = diff(B_CG_vy)./diff(t);
54 B_CG_a = sqrt(B_CG_ax.^2 + B_CG_ay.^2);
55 C_CG_ax = diff(C_CG_vx)./diff(t);%accn of COM of rocker
56 C_CG_ay = diff(C_CG_vy)./diff(t);
57 P2_ax = diff(P2_vx)./diff(t);%accn of P2
58 P2_ay = diff(P2_vy)./diff(t);
59 P3_ax = diff(P3_vx)./diff(t);%accn of P3
60 P3_ay = diff(P3_vy)./diff(t);
61
62 %% ANG. VELOCITIES
63 for i = 1:1:150
64 omega_3(i) = (P3_vy(i) - P2_vy(i))./(P3_x(i+1)-P2_x(i+1));%angular
       vel of coupler
65 omega_4(i) = (P3_vx(i))./(-P3_y(i+1));%angular vel of rocker
66 end
67
68 %% ANG. ACCNS
69 alpha_3 = diff(omega_3)./diff(t);%angular accn of coupler
70 alpha_4 = diff(omega_4)./diff(t);%angular accn of rocker
71
72 %% FORCE ANALYSIS
```

```
73
74 M_A = 0.79;M_B =1.02;M_C=2.18;%masses of links
75 I_A=40;I_B=155;I_C=311.96;%MOI of links about their COM
76 Solution=[];
77 for i = 1:1:149
78 R_mat = [1 0 1 0 0 0 0 0 0;...
79     0 1 0 1 0 0 0 0 0;...
80     A_CG_y(i+2) -A_CG_x(i+2) (A_CG_y(i+2)-P2_y(i+2)) (P2_x(i+2)-
     A_CG_x(i+2)) 0 0 0 0 1;...
81     0 0 -1 0 1 0 0 0 0;...
82     0 0 0 -1 0 1 0 0 0;...
83     0 0 (P2_y(i+2)-B_CG_y(i+2)) (-P2_x(i+2)+B_CG_x(i+2)) (-P3_y(i+2)+
     B_CG_y(i+2)) (P3_x(i+2)-B_CG_x(i+2)) 0 0 0;...
84     0 0 0 0 -1 0 1 0 0;...
85     0 0 0 0 0 -1 0 1 0;...
86     0 0 0 0 (P3_y(i+2)-C_CG_y(i+2)) (-P3_x(i+2)+C_CG_x(i+2)) (C_CG_y(
     i+2)) (-35-C_CG_x(i+2)) 0];
87
88 RHS = [M_A*A_CG_ax(i) - 1*M_A*980*cos(30*pi/180); M_A*A_CG_ay(i) - 1*
     M_A*980*sin(30*pi/180); 0;...
89     M_B*B_CG_ax(i) - 1*M_B*980*cos(30*pi/180); M_B*B_CG_ay(i) - 1*M_B
     *980*sin(30*pi/180);I_B*alpha_3(i);...
90     M_C*C_CG_ax(i) - 1*(M_C+1*7)*980*cos(30*pi/180) + 2*3.5*alpha_4(i
     )*sin(alfa(i)+beta(i)); M_C*C_CG_ay(i) - 1*(M_C+1*7)*980*cos(30*pi
     /180) - 7*3.5*alpha_4(i)*sin(alfa(i)+beta(i));...
91     I_C*alpha_4(i)+7*3.5*3.5*alpha_4(i)+ 1*7*980*3.5*sin(alfa(i)+beta
     (i))];
92
93 %Sol(i) = [F12x(i); F12y(i); F32x(i); F32y(i); F43x(i); F43y(i); F14x
     (i); F14y(i); T(i)];
94 Sol = inv(R_mat)*RHS;
95 Solution = [Solution Sol];%storing solutions in arrays
96 end
97
98 %% PLOT
99 for i=1:length(t)
100
101    ani = subplot(2,1,1);
102    P1_circle = viscircles(P1',0.05);
103    P2_circle = viscircles(P2(:,i)',0.05);
```

```
104    P3_circle = viscircles(P3(:,i)',0.05);
105    P4_circle = viscircles(P4',0.05);
106
107    A_bar = line([P1(1) P2(1,i)],[P1(2) P2(2,i)]);
108    B_bar = line([P2(1,i) P3(1,i)],[P2(2,i) P3(2,i)]);
109    C_bar = line([P3(1,i) P4(1)],[P3(2,i) P4(2)]);
110
111    axis(ani,'equal');
112    set(gca,'XLim',[-50 50],'YLim',[-50 50]);
113
114    str1 = 'P3';
115    str2 = ['Time elapsed: '  num2str(t(i)) ' s'];
116    P3_text = text(P3(1,i),P3(2,i)+0.4,str1);
117    Time = text(-2,6,str2);
118    pause(0.005);
119    if i<length(t)
120     delete(P1_circle);
121     delete(P2_circle);
122     delete(P3_circle);
123     delete(P4_circle);
124     delete(A_bar);
125     delete(B_bar);
126     delete(C_bar);
127     delete(P3_text);
128     delete(Time);
129     vel = subplot(2,1,2);
130     plot(vel,t(1:i),(Solution(9,1:i)));
131     set(vel,'XLim',[0 3]);
132     xlabel(vel, 'Time (s)');
133     ylabel(vel, 'Torque(kg.cm2/s2)');
134     title(vel,'Torque');
135     grid on;
136    end
137
138    end
```

BIBLIOGRAPHY

[1] J. H. Bargren et al. “Mechanical tests on the tibial components of non-hinged knee prostheses”. In: *Journal of Bone and Joint Surgery - Series B* (1978). ISSN: 0301620X. DOI: 10.1302/0301-620x.60b2.659476.

[2] Wujing Cao et al. “Design and Evaluation of a Novel Microprocessor-Controlled Prosthetic Knee”. In: *IEEE Access* (2019). ISSN: 21693536. DOI: 10.1109/ACCESS.2019.2957823.

[3] Danielle Collins. *When is static load capacity important?* 2016. URL: https://www.linearmotiontips.com/when-is-static-load-capacity-important/.

[4] D. Datta and J. Howttt. “Conventional versus microchip controlled pneumatic swing phase control for trans-femoral amputees: User’s verdict”. In: *Prosthetics and Orthotics International*. 1998. DOI: 10.3109/03093649809164474.

[5] Bill Dupes. “Prosthetic Knee Systems”. In: *Coalición de amputados de América* (2004).

[6] F. Ferryanto et al. “Design Modification of an Affordable Prosthetic Knee Based on DFMA and Static Analysis”. In: *Proceedings of 2017 5th International Conference on Instrumentation, Communications, Information Technology, and Biomedical Engineering, ICICI-BME 2017*. 2018. ISBN: 9781538634554. DOI: 10.1109/ICICI-BME.2017.8537726.

[7] Huiqun Fu et al. “A novel prosthetic knee joint with a parallel spring and damping mechanism”. In: *International Journal of Advanced Robotic Systems* (2016). ISSN: 17298814. DOI: 10.1177/1729881416658174.

[8] Steven A. Gard. “The Influence of Prosthetic Knee Joints on Gait”. In: *Handbook of Human Motion*. 2016. DOI: 10.1007/978-3-319-30808-1{_}75-1.

[9] M. P. Greene. “Four bar linkage knee analysis”. In: *Orthotics and Prosthetics* (1983). ISSN: 00305928.

[10] Marie Claude L. Grisé, Christiane Gauthier-Gagnon, and Georges G. Martineau. “Prosthetic profile of people with lower extremity amputation: Conception and design of a follow-up questionnaire”. In: *Archives of Physical Medicine and Rehabilitation* (1993). ISSN: 00039993. DOI: 10.1016/0003-9993(93)90014-2.

[11] Genki Hisano et al. “Factors associated with a risk of prosthetic knee buckling during walking in unilateral transfemoral amputees”. In: *Gait and Posture* (2020). ISSN: 18792219. DOI: 10.1016/j.gaitpost.2020.01.002.

[12] J. Steen Jensen and W. Raab. “Clinical field-testing of ATLAS prosthetic system for trans-femoral amputees”. In: *Prosthetics and Orthotics International* (2003). ISSN: 03093646. DOI: 10.3109/03093640309167977.

[13] Dewen Jin et al. “Kinematic and dynamic performance of prosthetic knee joint using six-bar mechanism”. In: *Journal of Rehabilitation Research and Development* (2003). ISSN: 07487711. DOI: 10.1682/JRRD.2003.01.0039.

[14] J. H. Kim and J. H. Oh. “Development of an above knee prosthesis using MR damper and leg simulator”. In: *Proceedings - IEEE International Conference on Robotics and Automation*. 2001. ISBN: 0780365763. DOI: 10.1109/ROBOT.2001.933191.

[15] Sittikorn Lapapong et al. “Finite element modeling and validation of a four-bar linkage prosthetic knee under static and cyclic strength tests”. In: *i-CREATe 2013 - International Convention on Rehabilitation Engineering and Assistive Technology, in Conjunction with SENDEX 2013*. 2013. DOI: 10.3402/jartt.v2.23211.

[16] Marcia W. Legro et al. “Prosthesis evaluation questionnaire for persons with lower limb amputations: Assessing prosthesis-related quality of life”. In: *Archives of Physical Medicine and Rehabilitation* (1998). ISSN: 00039993. DOI: 10.1016/S0003-9993(98)90090-9.

[17] Yong Guang Liu and Jian Sun. “Design of display retractile testing mechanism based on crank rocker”. In: *Proceedings of the 2015 10th IEEE Conference on Industrial Electronics and Applications, ICIEA 2015*. 2015. ISBN: 9781467373173. DOI: 10.1109/ICIEA.2015.7334227.

[18] Lorin P. Maletsky and Ben M. Hillberry. “Simulating dynamic activities using a five-axis knee simulator”. In: *Journal of Biomechanical Engineering* (2005). ISSN: 01480731. DOI: 10.1115/1.1846070.

[19] Benjamin F. Mentiplay et al. “Lower limb angular velocity during walking at various speeds”. In: *Gait and Posture* (2018). ISSN: 18792219. DOI: 10.1016/j.gaitpost.2018.06.162.

[20] J. Nogi et al. “Load testing of geometric and polycentric total knee replacements”. In: *Clinical Orthopaedics and Related Research* (1976). ISSN: 0009921X. DOI: 10.1097/00003086-197601000-00026.

[21] S. Ostermeier, C. Hurschler, and C. Stukenborg-Colsman. “Quadriceps function after TKA - An in vitro study in a knee kinematic simulator”. In: *Clinical Biomechanics* (2004). ISSN: 02680033. DOI: 10.1016/j.clinbiomech.2003.11.006.

[22] Physiopedia. *Prosthetic Knees*. 2020. URL: https://www.physio-pedia.com/index.php?title=Prosthetic_Knees&oldid=229249.

[23] Stanley Plagenhoef, F. Gaynor Evans, and Thomas Abdelnour. “Anatomical Data for Analyzing Human Motion”. In: *Research Quarterly for Exercise and Sport* (1983). ISSN: 21683824. DOI: 10.1080/02701367.1983.10605290.

[24] J E Shigley, C R Mischke, and R G Budynas. “Shigle’s mechanical engineering design - 9th Ed.” PhD thesis. 2002. ISBN: 9780070568990. DOI: 10.1007/s13398-014-0173-7.2. arXiv: 9809069v1 [gr-qc].

[25] Sugiyanto et al. “Stress analysis of four-bar linkage transfemoral prosthetic in gait cycle”. In: *International Journal of Applied Engineering Research* (2017). ISSN: 09739769.

[26] Gokce Yildirim et al. “Next generation knee replacements: A new approach to replicate the function of the ACL”. In: *Proceedings of the ASME Summer Bioengineering Conference 2007, SBC 2007*. 2007. ISBN: 0791847985. DOI: 10.1115/sbc2007-176201.